COMBUSTION SCIENCE AND TECHNOLOGY
2018, VOL. 190, NO. 8, 1472–1487
https://doi.org/10.1080/00102202.2018.1452130

Taylor & Francis
Taylor & Francis Group

Combined experimental and numerical study of ethanol laminar flame extinction

W. Wang, A. E. Karataş, C. P. T. Groth, and Ömer. L. Gülder

Institute for Aerospace Studies, University of Toronto, Toronto, Ontario, Canada

ABSTRACT

Extinction strain rates of ethanol at atmospheric pressure were investigated in laminar counter-flow diffusion flames as a function of nitrogen dilution through both experiment and two-dimensional axisymmetric full domain numerical analysis. An opposed-jet burner configuration with straight-tube fuel and air nozzles and having two different design nozzle exit flow profiles was used in the experiments. An advanced numerical solution algorithm, which makes use of a block-based parallel implicit finite-volume scheme, was used to obtain the corresponding simulation results. A comparison of the numerical results for two different chemical kinetic mechanisms helped to identify key factors affecting the flame extinction. While the predicted values over estimated the experimentally observed global strain rate extinction limits, the general trends and nozzle flow profiles were well captured. The local strain rates near extinction were also examined numerically and shown to be independent of the nozzle velocity flow profile and a fundamental property of the reactants. The experimental data from the present study were also compared to previous measurements and good agreement was demonstrated. The predicted nozzle exit and axial velocity flow profiles arising from the two-dimensional analysis were examined and limitations of conventional one-dimensional counter-flow analyses were highlighted.

ARTICLE HISTORY
Received 21 September 2017
Revised 9 January 2018
Accepted 19 January 2018

KEYWORDS
Biofuels; Ethanol; Flame Extinction; Extinction Strain Rate; Counter-Flow Laminar Diffusion Flames

Introduction and motivation

Ethanol is one of the more important liquid biofuels for transportation and stationary gas turbines. It is attractive as a low-pollution and renewable fuel (Saxena and Williams, 2007) and is already widely used in the world as a fuel extender, octane enhancer, and oxygen-additive in or as a replacement for gasoline (Li et al., 2007). The vast majority of cars in North America today are running on blends of up to 10% ethanol (Flavin et al., 2006).

In spite of ethanol's widespread use as a biofuel (Li et al., 2007; Saxena and Williams, 2007), there have been only a limited number of studies of its flame extinction properties. Extinction strain rate is an important characteristic of diffusion flames (Williams, 2001) and is a measure of fuel flammability and the susceptibility of flames to suppression. The only experimental extinction study with ethanol in non-premixed counter-flow diffusion flames that the authors are aware of is by Seshadri (2005) and Seiser et al. (2007). Furthermore, most, if not all, of the few related numerical studies for ethanol have been

CONTACT C. P. T. Groth groth@utias.utoronto.ca; Ö. L. Gülder ogulder@utias.utoronto.ca University of Toronto Institute for Aerospace Studies, 4925 Dufferin Street, Toronto, Ontario M3H 5T6, Canada

Color versions of one or more of the figures in the article can be found online at www.tandfonline.com/gcst.

conducted using the standard or traditional one-dimensional (1D) analysis tools. The goal of the present work is therefore to re-examine the structure of counter-flow non-premixed diffusion flame and extinction limits for ethanol both experimentally and through the use of an advanced computational solution algorithm on two-dimensional (2D) axisymmetric domains, and thereby gain greater insight into the behaviour and extinction process for non-premixed ethanol flames.

Counter-flow burner and experimental methodology

Strain rate is representative of the residence time of reactants in the reaction zone and small aerodynamic time scales are indicative of elevated strain rates. In a counter-flow laminar diffusion flame, the aerodynamic strain rate is defined in terms of the gradient of the axial velocity component, $\partial u/\partial x$, where u is the axial component of velocity and x is the position coordinate in the axial direction along the burner centre line. The convention within literature is to express the local strain rate, a_l, as

$$a_l = \left.\frac{\partial u}{\partial x}\right|_{\max} \tag{1}$$

just prior to the thermal mixing layer of the flame on either the air or fuel side, depending on the location of the flame with respect to the stagnation plane (Egolfopoulos et al., 1989; Sarnacki et al., 2012; Yu et al., 1986). The stoichiometric mixture fraction, Z_{st} (Du and Axelbaum, 1995), which can be used to position the flame with respect to the stagnation plane in Z (mixture fraction) space is given as (Xia and Axelbaum, 2013)

$$Z_{st} = \left(1 + \frac{Y_R W_O \nu_O}{Y_O W_R \nu_R}\right)^{-1} \tag{2}$$

where Y, W, and ν are mass fractions, molecular weight and stoichiometric coefficient, respectively, and the subscripts R and O denote the reactant and oxidizer chemical species in fuel and air streams, respectively. The stagnation plane is located at $Z_{st} = 0.50$, and thus flames located on the air and fuel side of the stagnation plane have values of $Z_{st} < 0.50$ and $Z_{st} > 0.50$, respectively.

In the absence of direct measures of a_l, the local strain rate can be approximated by the global strain rate as first formulated by Seshadri and Williams (1978), which is a function of nozzle exit bulk flow velocities, nozzle separation, and the densities of fuel and air streams. Potential flow is assumed within the counter-flow geometry which predicts a linear deceleration of the axial component of velocity as the gases approach the stagnation plane. Factoring in a correction for the density differences of the fuel and air streams, the global strain rate, a_g, can be expressed as

$$a_g = \frac{2V_A}{L}\left[1 + \frac{V_F}{V_A}\left(\frac{\rho_F}{\rho_A}\right)^{1/2}\right] \tag{3}$$

where L, V, and ρ denotes nozzle separation distance, nozzle bulk flow velocity, and density respectively, and the subscripts F and A denote fuel and air streams, respectively.

The experimental apparatus used herein consists of a single counter-flow burner, designed specifically to handle high flow conditions (Wang, 2014). The burner includes two identical nozzle assemblies, each with inner and concentric nozzles (Figure 1). The inner nozzles supply the fuel mixture (fuel diluted with nitrogen) and air streams from the lower and upper assemblies, respectively, while the outer nozzles of both assemblies supply co-flow nitrogen, which isolates the flame from the ambient atmosphere. Two interchangeable inner nozzle configurations are available for the counter-flow burner. One configuration of the inner nozzle (parabolic profile configuration as depicted on right side of figure) has smooth bore tubes, for which a parabolic velocity distributions are expected at the nozzle exits in accordance with laminar pipe flow theory. However, as will be shown, in reality the parabolic configuration may result in somewhat different inflow conditions at the nozzle exit plane that are subject to variations depending on the pressure field generated by the opposed jets. The second configuration (uniform profile configuration as depicted on left side of figure) incorporates a sintered metal matrix 5.1 mm upstream of the nozzle exit plane, with the intention of creating uniform or top-hat velocity profiles at the nozzle exit planes. As will also be shown, the matrix is however

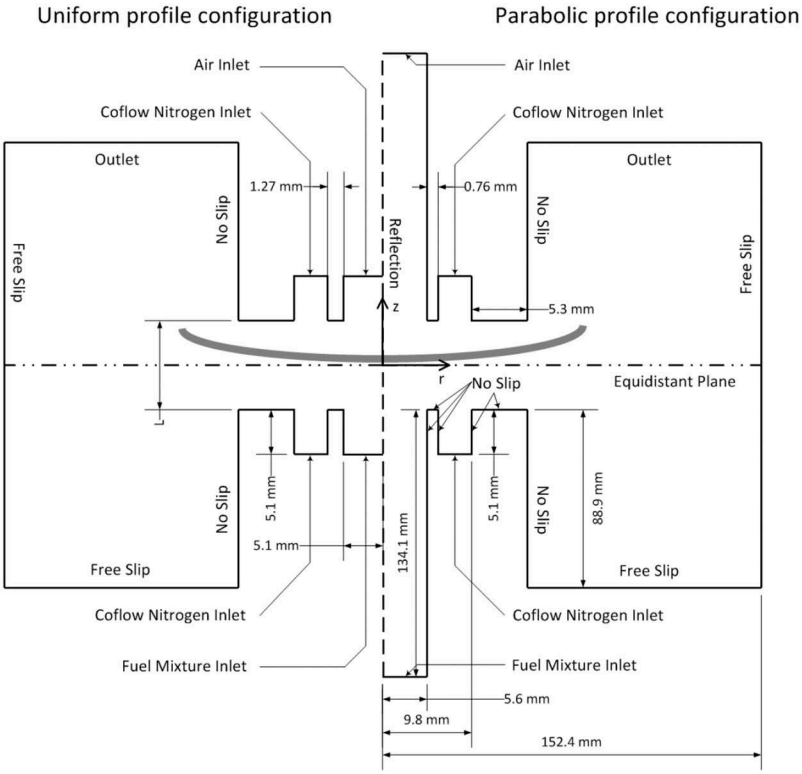

Figure 1. Schematic diagram (not to scale) of 2D axisymmetric counter-flow burner and computational domain and boundary conditions used in numerical simulations showing both uniform (left) and parabolic (right) profile configurations (identical dimensions in both configurations are labelled only on the right).

not sufficient to ensure idealized uniform profiles of fuel and air at the nozzle exits. Similar sintered metal matrix meshes are fitted in the outer nozzles used to supply the co-flow nitrogen so as to provide similar uniform inflow velocity profiles in both burner configurations. The radii of the inner nozzles are 5.6 mm and 5.1 mm, and tube wall thicknesses are 0.76 mm and 1.27 mm, respectively, for the so-called parabolic and uniform profile configurations. The nozzle separation distance, L, was maintained at 10.2 mm, such that the burner L/D ratio was either 0.91 or 1, depending on the configuration of the inner nozzles, where D represents the inner nozzle diameter. The radius and tube wall thickness of the outer nozzle are 9.8 mm and 5.3 mm, respectively. A ceramic glass enclosure houses the burner, allowing visual and optical access to the flame.

The dilution and evaporation of liquid ethanol was accomplished by using a fuel vaporizer system constructed in-house. A syringe pump was used to feed the liquid fuel into a heated evaporation chamber. The fuel evaporation and mixing chamber was a small volume (about 4×10^{-5} m^3) high-pressure vessel. Liquid fuel and heated nitrogen carrier gas (also serving as the dilution gas) were injected into this heated evaporation chamber through a co-flow injector. The fully evaporated and diluted fuel was then directed to the burner through a heated tube set to 473 K so as to prevent condensation.

The strain rate was controlled by adjusting the flow rates of fuel mixture and air streams using flow controllers with calibrated accuracy within 1%. A stable flame was first established near but below the extinction limit and the experiments were then carried out by gradually applying small or incremental increases to the flow strain rate. Due to the fuel vaporizer setup, it was desirable to keep the liquid ethanol flow rate constant to prevent sudden changes in temperature (Wang, 2014). Thus, the increase in strain rate was accomplished by sequentially increasing the dilution nitrogen and air streams, respectively, while maintaining a constant liquid ethanol flow rate (effectively decreasing the fuel mole fraction as strain rate increases), until the flames were extinguished. At each step of this process, the momentum balance of the fuel mixture and air streams were maintained. Additionally, the flame was monitored and allowed about 30 seconds to stabilize between each step. Each step change in strain rate was maintained at about 1–5% of the global extinction strain rate and the experiments were repeated multiple times for each fuel flow rate. In this way, the extinction limits were accurately established.

Numerical simulation of counter-flow burner and flame extinction

Finite-volume solution method

The computational framework developed by Charest et al. (2010) for the prediction of laminar reactive flows with complex chemistry, non-gray radiative heat transfer, and soot was applied to the prediction of the counter-flow diffusion flames of interest herein. This numerical modelling tool was specifically developed for use with large multi-processor parallel computers and its capabilities have been previously demonstrated in a number of recent studies of laminar co-flow diffusion flames under both high pressure and low gravity conditions (Charest et al., 2010, 2011a, 2011b, 2011).

The framework solves the conservation equations for a multi-component, compressible, reactive, gaseous mixtures. Soot formation/oxidation and radiation were not included here since these effects are expected to be small for the ethanol fuel and atmospheric pressures

of interest. The governing equations are solved using a finite-volume method previously developed by Groth and co-workers (Charest et al., 2010; Gao and Groth, 2006; Gao et al., 2011; Sachdev et al., 2005). The scheme makes use of piece-wise limited linear reconstruction and an approximate Riemann solver to determine numerical values of the inviscid fluxes (Roe, 1981) and second-order diamond-path method for the viscous fluxes. Low-Mach-number preconditioning is applied to reduce the excessive dissipation and numerical stiffness of the discretized system and permit accurate solution for the low-speed flames of interest (Weiss and Smith, 1995). The solution of the fully-coupled non-linear equations resulting from the finite-volume discretization procedure are relaxed to steady-state using a parallel implicit algorithm which uses a matrix-free Newton–Krylov method. Thermodynamic/transport properties and gas-phase reaction rates are evaluated using CANTERA (Goodwin, 2003).

The simulations were performed using a chemical kinetic mechanism for ethanol combustion consisting of 39 species and 238 reactions developed by Li et al. (2007), referred to here as the Princeton mechanism, and a reduced mechanism based on the Princeton model consisting of 29 species and 154 reactions that was recently developed by Akih-Kumgeh (2013). While other detailed mechanisms, such as the 56 species, 383 reaction mechanism of Marinov (1999), and the more recent 57 species, 288 reaction mechanism of Saxena and Williams (2007), have been developed, they were not considered here.

Axisymmetric computational domain and grids

The parabolic profile configuration created some uncertainty regarding the specification of the inflow velocity at the nozzle exit planes of the inner nozzles. It was found that applying idealized parabolic velocity distributions at the inflow boundaries near the nozzle exits produced poor predictions of extinction strain, particularly at high flow rates (Wang, 2014). Furthermore, the experimental study of Vagelopoulos and Egolfopoulos (1998) has shown that the nozzle velocity flow distribution is affected by the radial pressure gradient created by the opposed jets and Sarnacki et al. (2012) later demonstrated in their experiments that the nozzle velocity flow distribution deviates from a parabolic profile as the strain rate is increased. Amantini et al. (2007) approached this problem by using the measured nozzle flow distribution as the numerical inflow boundary conditions at the nozzle exit plane. However, this approach is heavily dependent on availability of experimental data which were not available here. To overcome this issue in the present study, a full 2D axisymmetric computational domain was used. The computational domain of the inner nozzles was extended upstream by 12 times their diameter and uniform inflow velocity distributions were imposed at these upstream boundaries. By including the additional upstream portions of the inner fuel and air stream nozzles within the computational domain for the parabolic configuration, the nozzle exit plane velocity distributions were computed directly as part of the simulation such that the predicted profiles match the pressure and flow conditions at the nozzle exits.

Conversely, the uniform profile configuration was modelled by simply applying uniform inflow velocity profiles at the locations of the sintered metal matrix within the nozzles just upstream of the exit plane. Note that it was found that the sintered metal matrix was unable to maintain ideal uniform profiles at the exit planes of the inner nozzles

(Wang, 2014), leading to generally poor agreement between numerical and experimental flow fields for elevated flow rates when studying various gaseous fuels. Nevertheless, it is felt that the present numerical setup for the uniform configuration should adequately approximate the experimental conditions at the metal matrix meshes as the flow rates necessary for the extinction of ethanol are relatively low in comparison to those required for the gaseous fuels of the previous study.

The computational domains adopted here are shown schematically in Figure 1 for both the parabolic and uniform profile configurations. The domain in each case is symmetrical along the equidistant plane and extends 152.4 mm radially. The nozzle radii, separation distance, tube thicknesses, and far-field domain boundaries are modelled precisely based on the burner geometry and exhaust enclosure of the experimental facility. The inner nozzles extend 134.1 mm and 5.1 mm upstream from nozzle exit plane for the parabolic and uniform configurations, respectively, while the outer nozzles extend just 5.1 mm upstream to the position of the sintered metal matrix. No-slip boundary conditions were applied at the nozzle tube walls while the far-field and lower boundaries of the domain were treated as free-slip boundaries. All tube walls were taken to have a fixed temperature of 300 K. The upper boundary of the domain serves as the flow outlet, where values of temperature, velocity, and species mass fraction were extrapolated from the interior of the domain while the pressure was specified and held at a fixed value. The compositions of the gaseous mixtures were specified at all inlet boundaries, along with the velocity and temperature, while the pressure was extrapolated from the interior of the domain. Uniform velocity and temperature profiles were specified for the air, fuel mixture, and co-flow nitrogen inlet boundaries, in all cases.

For the parabolic profile burner configuration, the computational mesh was subdivided into 180 cells and 18 blocks in the radial and 672 cells and 42 blocks in the axial directions, respectively. The resulting structured but non-uniformly spaced mesh consisted of 92,160 quadrilateral cells within 576 blocks. For the uniform profile configuration, the computational mesh was subdivided into 180 cells and 18 blocks in the radial and 640 cells and 40 blocks in the axial direction. This produced a mesh consisting of 81,920 cells and 512 blocks. In both cases, the cells were clustered radially towards the centre line and axially towards the equidistant plane so as to provide higher resolution for regions containing the flow. The vertical mesh spacing between the inner nozzles was approximately 35 μm, while the spacing was approximately 140 μm in the radial direction. The computational grid used in the simulations of the parabolic profile burner configuration is depicted in Figure 2, showing the distribution of both the grid blocks and quadrilateral cells. The mesh used for the simulation of the uniform profile burner was very similar. A systematic mesh refinement study was performed to ensure that the resolution of these two meshes were sufficient for the purposes of the present extinction studies (Wang, 2014).

Procedure for computation of extinction limits

Numerical extinction was determined in a manner similar to that adopted in the experiments. A converged steady counter-flow flame solution was first established well below the expected extinction strain limit. The converged solution was then used as an initial estimate or starting solution for determining a new solution at a higher strain rate, with the higher strain rate imposed by simply modifying the inflow boundary conditions and

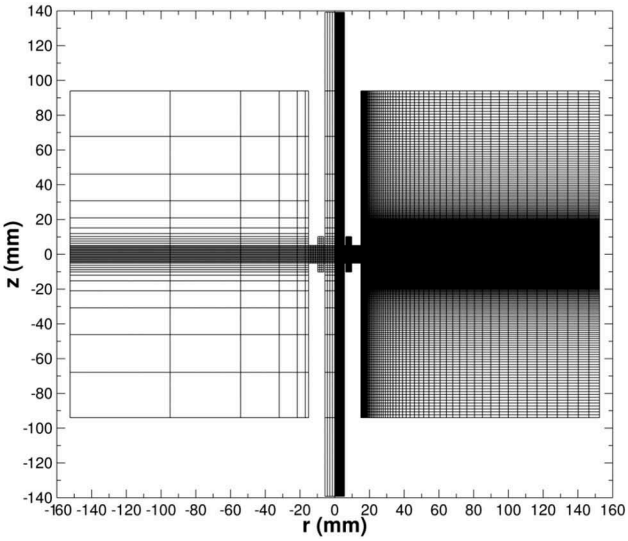

Figure 2. Computational mesh used in 2D axisymmetric simulations of the counter-flow burner for parabolic profile configuration showing the computational blocks of the multi-block grid (left), as well as the distribution of the computational cells (right); grid consists of 576 blocks and 92,160 quadrilateral cells.

prescribing higher bulk flow velocities in the fuel and air stream nozzles. This process was repeated in an iterative manner until the numerical solution no longer supported a flame and a precise value for the extinction strain rate was established. The final step size increases in the global strain rate at extinction were kept sufficiently small, as summarized in Table 1, to ensure that the error in the computed extinction strain rate was below 3%.

Analyses and comparison of experimental and numerical results

Assessment of chemical kinetic mechanisms

Prior to considering the complete set of ethanol extinction results, an assessment is made of the relative effectiveness of the chemical kinetic models considered in this study for the prediction of extinction strain. In particular, numerical results obtained using the full chemical kinetic mechanism of Li et al. (2007) (referred to as the Princeton mechanism in the figures), and the reduced version of the Li et al. mechanism developed by Akih-Kumgeh (2013) (referred to as the reduced Princeton mechanism in the figures) are compared. The comparisons of the two mechanisms were conducted for the parabolic profile burner configuration.

To begin with, the predicted numerical values of the global extinction strain rate, $(a_g)_e$, for both the full and reduced Princeton mechanisms are shown in Figure 3(a) as a

Table 1. Strain rate step sizes used in the computation of the flame extinction limit.

a_g (s^{-1})	≤ 200	≤ 500	≤ 1000	≥ 1001
Step size (s^{-1})	2	5	10	20

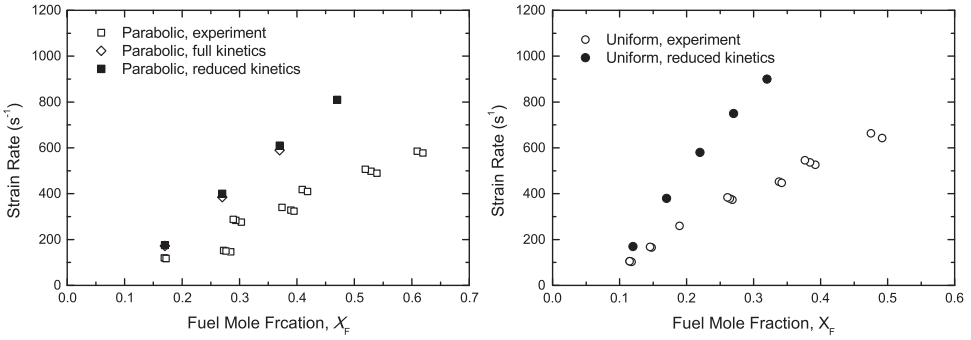

(a) Parabolic profile burner. (b) Uniform profile burner.

Figure 3. Comparison of experimental (white symbol) and numerical (black symbol) global extinction strain rates of ethanol-air counter-flow diffusion flames for (a) parabolic and (b) uniform profile burner configurations.

function of the fuel mole fraction, X_F. Ignoring for the moment the comparisons to experimental values, it can be seen that the predicted global extinction limits for both mechanisms are virtually identical, with those of the reduced mechanism being marginally higher than those of the full model.

The predicted 2D axisymmetric flame structures obtained using the two mechanisms are further compared in Figure 4, where the solutions of the full and reduced mechanisms are given on the left and right sides of the figure, respectively. The figure depicts the computed temperature distributions and flow streamlines for a diluted ethanol flame with the parabolic configuration for $X_F = 0.37$ and $a_g = 580\ s^{-1}$ just prior to extinction. It is quite evident that the resulting flame structure and flow field provided by each mechanism are virtually identical.

More detailed comparisons of the predictions of two mechanisms for a diluted ethanol flame with the parabolic configuration for $X_F = 0.37$ and $a_g = 580\ s^{-1}$ just prior to

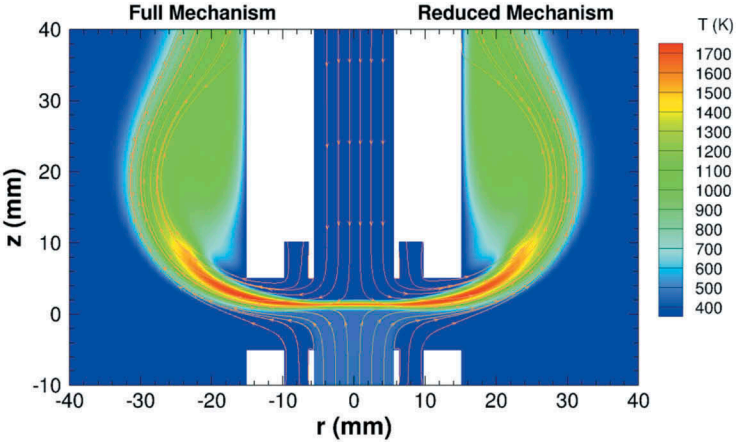

Figure 4. Comparison of predicted 2D axisymmetric flame solutions obtained using the full Princeton (left) and reduced Princeton chemical kinetic (right) mechanisms for parabolic profile burner configuration with ethanol fuel, $X_F = 0.37$, and $a_g = 580\ s^{-1}$.

extinction are afforded by Figure 5, where centre-line solution profiles are depicted. While there are no noticeable differences in the predictions of the distributions of temperature, axial velocity, and fuel and air species mass fractions along the axis of symmetry (the overall flame structure provided by each mechanism are virtually identical), small differences in major combustion products and radicals distributions can be observed between the two mechanisms. In particular, there is a noticeably higher concentration of CO_2 in the combustion products, as well as OH, O, and H radicals predicted by the reduced mechanism. This is indicative of a more active flame that is expected to be slightly more resistant to extinction, as indicated in the results of Figure 3(a). As both mechanisms appear to provide similar results in terms of flame structure and extinction properties, for computational efficiency, the reduced mechanism was used exclusively in obtaining the remainder of the numerical results reported herein.

Comparison of measured and predicted global strain rate

Returning to Figure 3, consider now the comparison of the experimentally measured and numerically predicted values of the global extinction strain rates for both the parabolic and uniform profile burner configurations. Firstly, it should be noted that experimental data in Figure 3(a) for the parabolic configuration shows a noticeable sudden jump in the otherwise nearly linear behaviour for strain rates in the range $a_g \approx 100$–200 s^{-1}. It is speculated that this is due to early extinction of the flames caused by the flow instabilities as previously reported by Wang (2014) for this burner geometry. These instabilities appear

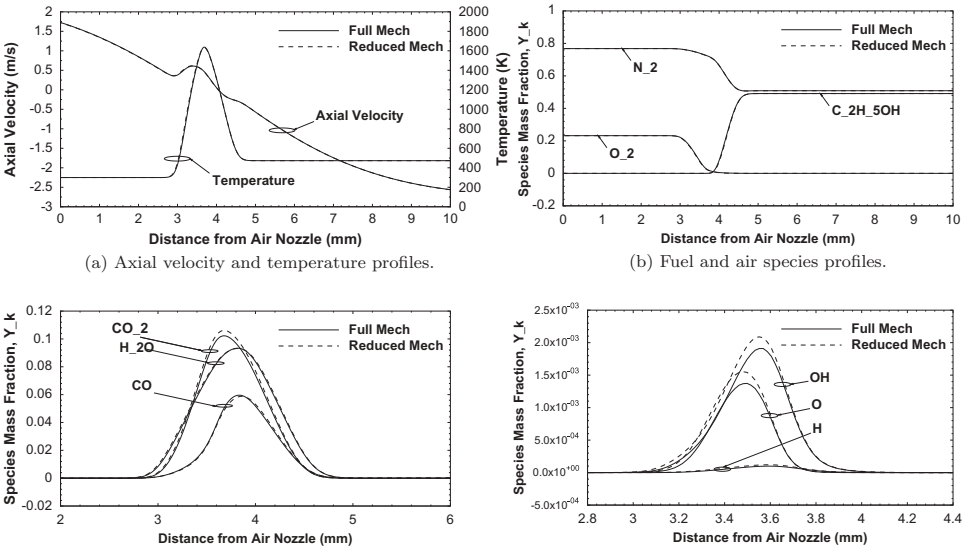

(a) Axial velocity and temperature profiles.

(b) Fuel and air species profiles.

(c) Profiles of major combustion products.

(d) Radical profiles.

Figure 5. Comparison of predicted centre-line solution profiles obtained using the full and reduced Princeton chemical kinetic mechanisms for parabolic profile burner configuration with ethanol fuel, $X_F = 0.37$, and $a_g = 580$ s^{-1}: (a) axial velocity and temperature profiles; (b) fuel and air species profiles; (c) profiles of major combustion products; and (d) profiles of radicals (note that axis scales are different on each sub-plot).

to arise from aerodynamic effects and are independent of fuel composition. It is also worth noting that the fuel and air nozzle flow Reynolds numbers are estimated to be well below the established limit for laminar flow in fully developed pipes for all of the extinction results shown in the figure.

From Figure 3, it is also evident that the numerical predictions of the extinction limits for both parabolic and uniform configurations significantly over-predict by as much as 70% the experimentally measured values. In spite of these quantitative discrepancies, the overall positive correlation between the global extinction strain rate and fuel mole fraction of the fuel mixture, as well as the differences between the two flow profiles, are reasonably well captured. The large numerical over-prediction of measured values for extinction strain is likely due to the limitation of the chemical kinetic mechanism, as both the full and reduced mechanisms were formulated without being specifically tuned to match the results of extinction studies. The differences between the measured and predicted values for the extinction strain may also be attributed to inaccuracies in the gas-phase models for the species and mixture transport coefficients. Note that it has been shown that even a small change in the concentrations of critical chemical species, such as OH in the reaction zone, can have a large effect on the global strain rate near extinction (Wang, 2014), indicating that extinction prediction is very sensitive to the production, transport, and destruction of these species.

Comparison of measured and predicted local strain rate

While the global strain rate at extinction can be defined using Eq. (3) for the flow conditions under which flame extinction occurs, the local extinction strain rate, as defined by Eq. (1), should be evaluated just prior to extinction, when the flame is still present. This is because the existence of the flame distorts and alters the velocity field. It is therefore desirable to determine the local strain rate as close to extinction as possible, in order to fairly compare local and global values of the extinction strain rates.

For ethanol, regardless of the dilution with nitrogen, it was found that $Z_{st} < 0.50$. Accordingly, the local strain rates were evaluated on the fuel mixture side of the flame. In each case, the local strain rates, $(a_l)_{ne}$, near extinction were evaluated numerically using the flame solutions at just one step in strain rate below the point of flame extinction as defined by Table 1. As this step size is less than 3% of the value of the global strain rate, this should represent an upper bound on the computed error in the local strain rate at the actual point of extinction.

Predicted values of the local near extinction strain rate and global strain rate at extinction for both burner configurations are compared to the present measured values of the global strain rate, as well as to other experimental and numerical results obtained by Seshadri (2005) and Seiser et al. (2007) (referred to here as Seshadri et al.). The global strain rates at extinction for the uniform profile are significantly higher than those of the parabolic profile for a given fuel mole fraction. However, it was also quite evident that the local strain rates near extinction are largely independent of flow profile, with minimal differences are seen for the different flow profiles. Furthermore, the global extinction strain rates for the parabolic profile provide significantly better approximations of local near extinction strain rates than those from the uniform profile. The observed numerical

results suggest that the local strain rate at the point of extinction are independent of nozzle configuration and flow field and is a fundamental chemical kinetic property of the reactants.

Comparisons to extinction results from other sources

Seshadri et al. (Seiser et al., 2007; Seshadri, 2005) have conducted experimental and numerical investigations on ethanol-air counter-flow diffusion flame extinction. The counter-flow diffusion flame burner used by Seshadri et al. has an inner diameter $D = 22.2$ mm and a separation $L = 10$ mm, thus the burner has $L/D = 0.45$. However, the fine wire screens were placed at both nozzle exits to minimize the tangential component of flow velocity and produce a plug flow (uniform) distribution, to a good approximation. Details of their burner can be found in Seiser et al. (2007, 1998), Seshadri (2005), Seshadri et al. (2009). Although the L/D ratio of their burner differ from the experimental setup of this study, their results are still relevant to the present findings as Wang (2014) has previously shown that the global strain rate at extinction for methane-air flames is largely independent of L/D in the case of uniform nozzle inflow profiles and for values of L/D in the range $0.5 \lesssim L/D \lesssim 1.0$. The local strain rates were however shown to be different by Wang (2014). In addition to these previous findings, qualitatively similar behaviours were observed by Won et al. (2010), where the global extinction strain rate were found to be repeatable between $0.45 \leq L/D \leq 0.635$ for their burner, which has honeycomb mesh installed 20 mm upstream of the nozzle exit to produce uniform nozzle inflow profile. Johnson et al. (2015) have also explored the validity of quasi-1D flow behaviour in counter-flow burner geometry as a function of burner diameter and nozzle separation and report related findings.

A comprehensive comparison of the extinction strain rates obtained in the present study, both experimentally and numerically, to those of Seshadri et al. (Seiser et al., 2007; Seshadri, 2005) is given in Figure 6. The data of Seshadri et al. were taken from Figure 2 of Seiser et al. (2007). It is evident that the experimental results for

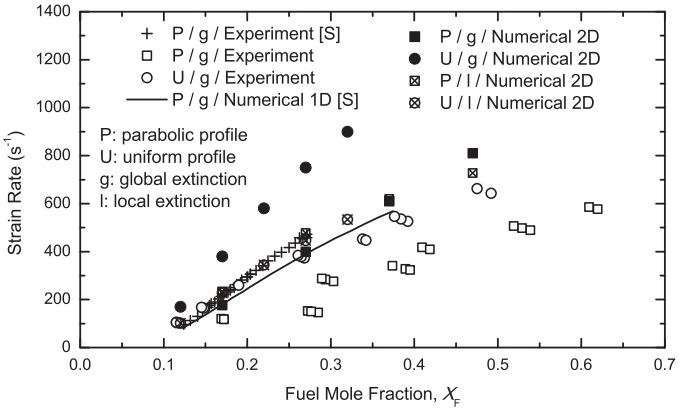

Figure 6. Summary of extinction strain results arising from current experimental and numerical studies of ethanol-air counter-flow diffusion flames along with a comparison to the previous results of Seshadri et al. (Seshadri, 2005; Seiser et al., 2007), where the latter is labelled [S] in the figure legend.

the uniform profile configuration of the present study closely match those of the previous study, especially for low flow rates at lower fuel mole fractions, indicating that the uniform or plug flow configuration described by Seshadri et al. is qualitatively similar to the uniform profile experimental configuration considered herein. However, at higher flow rates, the results appear to deviate slightly from the data of Seshadri et al., possibly due to the differences in burner design. The burner used in the present study imposes a uniform velocity distribution with the introduction of a metal mesh at 5.1 mm upstream of the nozzle exit while the burner of Seshadri et al. does so immediately at the nozzle exit. The L/D ratios are also different for both burners. Furthermore, it is known that the burner used in the present work does not maintain idealized uniform velocity profiles at high flow rates (Wang, 2014). It is noted that the experimental results of Seshadri et al. cover somewhat narrower ranges of flow rates and fuel mole fractions than the wider and higher ranges considered here.

As shown earlier, the 2D axisymmetric numerical solutions of global strain rate at extinction conducted in the present work significantly over-predicts by about 70% when compared to the global strain rates at extinction measured during experiments. However, the 1D numerical solution of Seshadri et al., which assumes uniform plug flow boundary conditions, seems to achieve better predictions, although under-predictions were seen at higher strain rates. Seshadri et al. used the chemical kinetic mechanism of Marinov (1999) that consists of 383 elementary reactions and 56 species for their study. It is believed that the use of chemical kinetic mechanisms and their associated transport models that are not specifically tuned for extinction studies contribute at least partially to the over-prediction. Aside from the different chemical kinetic mechanisms, it should be noted that the 1D numerical solution of Seshadri et al. may not accurately capture the multi-dimensional aspects of extinction process in a counter-flow diffusion flame burner as is possible with the 2D axisymmetric full domain numerical solution method used in the current study. One such multi-dimensional effect is the prediction of opposed-jet nozzle exit plane flow distributions, examined in detail by a few previous experimental studies (Korusoy and Whitelaw, 2001; Sarnacki et al., 2012), which indicated the importance of the nozzle flow distributions on flame extinction behaviour. It has been shown by Wang (2014) in other previous 2D full-domain axisymmetric numerical solutions that the nozzle velocity distributions change as a function of flow rate due the influence of pressure gradients created by the opposed-jet and that the nozzle exit plane flow distributions can differ significantly for the idealized expectations of the two nozzle configurations examined here as a function of the flow rate. Wang (2014) has also shown that non-zero velocity gradients can exist at the nozzle exits, especially at higher flow rates. See also the numerical results for ethanol below in the section to follow. These observations suggest limitations of 1D and even 2D numerical simulations that apply idealized inflow velocity at the nozzle exit and artificially force a zero velocity gradient or make such analyses very dependent on experimental measurements to establish the correct inflow boundary conditions for the simulations. It is likely that the under-predictions by Seshadri et al. at elevated flow rates were caused by the deviation from the plug flow distribution in experiments not captured in their 1D numerical solutions.

Lastly, it is noted that the similarity between the predicted local near extinction strain rates and experimental global extinction strain rates for both the parabolic profile results of the present work and the results of Seshadri et al. are likely fortuitous, since it has been established that global strain rates do not approximate well the local strain rates for the uniform profile configuration of this burner (Wang, 2014).

Multi-dimensional flame structure

The 2D numerical solution method used here permitted an examination of the reactive flow field over the entire computational domain and thus provided useful insight into the multi-dimensional structure and behaviour of the counter-flow flames. Nozzle exit plane velocity profiles of opposed jets have been the subject of several previous experimental studies (Korusoy and Whitelaw, 2001; Sarnacki et al., 2012). These studies indicated the importance of the resulting velocity profile on flame extinction behaviour. However, there have been very few multi-dimensional numerical studies on this subject. Very recently, Johnson et al. (2015) have performed an investigation of multi-dimensional effects in counter-flow burners and assessed requirements for the validity of quasi-1D theory.

While the nozzle exit plane velocity flow profiles can be investigated for either the fuel or oxidized nozzle of a counter-flow burner, it is customary in literature to study the behaviour from the air side. Predicted normalized axial velocity profiles of the air at the nozzle exit plane corresponding to near extinction ethanol-air counter-flow diffusion flames studied here are presented in Figure 7 for both the parabolic and uniform burner configurations. The idealized uniform and parabolic velocity profiles are also shown in the figure for comparison. From the results of this figure, it is quite evident that the predicted nozzle exit-plane velocity profiles are strongly dependent on flow rate. As the flow rate is increased, the influence of pressure forces created by the opposed jet flow causes the velocity profiles to deviate significantly from the idealized distributions. An examination of the predicted centre-line axial velocity distributions of Figure 8 also reveals that there are significant variations in the centre-line velocity and non-zero velocity gradients are

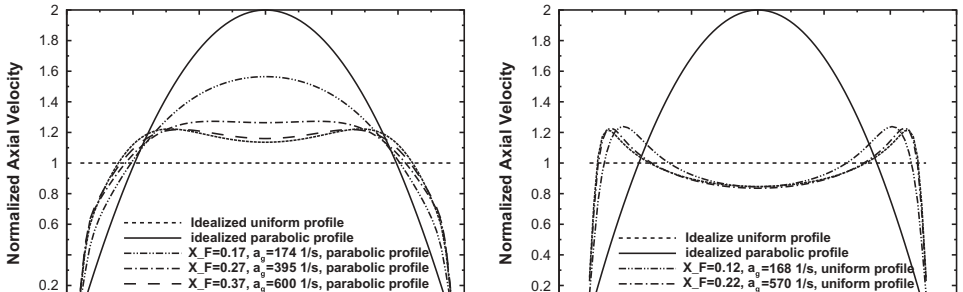

(a) Parabolic profile burner. (b) Uniform profile burner.

Figure 7. Air nozzle exit plane velocity flow profile for various dilution fractions and global strain rates for (a) parabolic and (b) uniform profile configurations near extinction of ethanol-air counter-flow diffusion flames.

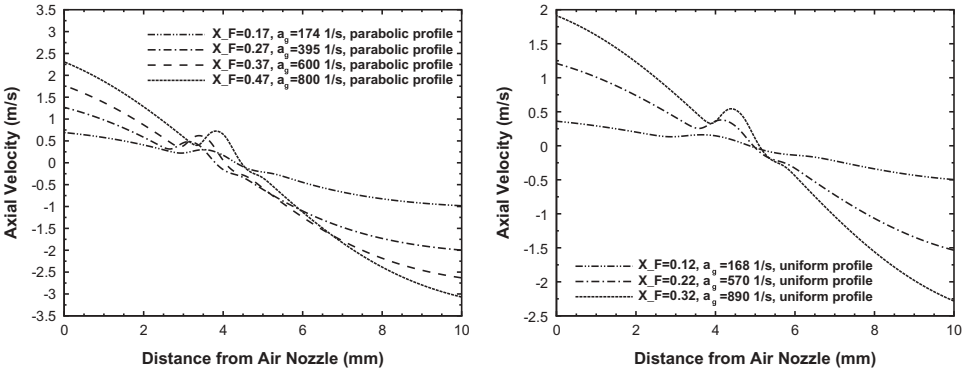

(a) Parabolic profile burner. (b) Uniform profile burner.

Figure 8. Axial centre-line velocity profile for various dilution fractions and global strain rates for (a) parabolic and (b) uniform profile configurations near extinction of ethanol-air counter-flow diffusion flames.

present at the nozzle exit plane, especially at higher flow rates. These findings further highlight the possible limitations of 1D and 2D numerical simulations based on imposed idealized inflow velocity profiles at the nozzle exit planes and the assumption that the velocity gradients in the axial direction are zero.

Conclusions

A combined experimental and numerical study of ethanol extinction in laminar counter-flow diffusion flames has been conducted. The 2D axisymmetric numerical solution method used here proved to be capable of reliable predictions of counter-flow flame structure and has allowed the identification of key factors affecting extinction. Although the global strain rate extinction limits for ethanol were somewhat over-predicted compared to the current measured values, the overall trends in the extinction behaviour were correctly captured. The relationship between global and local strain rates as a function of flow rate was investigated numerically. The predicted local strain rate at extinction was shown to be independent of the burner nozzle configuration and a fundamental property of the reactants. Furthermore, the global strain rate arising from the parabolic profile burner configuration was shown to provide superior agreement with and thus a good estimate of the local strain rate as compared to that provided by its uniform profile counterpart. Finally, due to the multi-dimensional aspects of opposed-jet burners highlighted in the study, caution should be exercised when comparing 1D numerical prediction of flame extinction to measured values of the global extinction strain rates. It is also recommended that the development and assessment of chemical kinetic mechanisms and their associated transport models for the prediction of flame extinction be carried out in conjunction with 2D full-domain simulations.

Funding

This work was supported by grants from the Ontario Research Fund Research Excellence (ORF-RE) programme and the Southern Ontario Smart Computing for Innovation Platform (SOSCIP) of the Province of Ontario. Computational resources for performing simulations reported in the paper were provided by the SOSCIP programme, as well as the SciNet High Performance Computing Consortium at the University of Toronto and Compute/Calcul Canada through funding from the Canada Foundation for Innovation (CFI) and the Province of Ontario, Canada.

References

Akih-Kumgeh, B. 2013 May. (Private correspondence).

Amantini, G., Frank, J.H., Smooke, M.D., and Gomez, A. 2007. Computational and experimental study of steady axisymmetric non-premixed methane counterflow flames. *Combust. Theor. Model.*, **11**, 47–72.

Charest, M.R.J., Groth, C.P.T., and Gülder, Ö. L. 2010. A computational framework for predicting laminar reactive flows with soot formation. *Combust. Theor. Model.*, **14**(6), 793–825.

Charest, M.R.J., Groth, C.P.T., and Gülder, Ö. L. 2011a. Effects of gravity and pressure on laminar co-flow methane-air diffusion flames at pressures from 1 to 60 atmospheres. *Combust. Flame.*, **158**(5), 860–875.

Charest, M.R.J., Groth, C.P.T., and Gülder, Ö. L. 2011b. Numerical study on the effects of pressure and gravity in laminar ethylene diffusion flames. *Combust. Flame.*, **158**(10), 1933–1945.

Charest, M.R.J., Joo, H.I., Groth, C.P.T., and Gülder, Ö. L. 2011. Experimental and numerical study of soot formation in laminar ethylene diffusion flames at elevated pressures from 10 to 35 atm. *Proc. Combust. Inst.*, **33**, 549–557.

Du, J., and Axelbaum, R.L. 1995. The effect of flame structure on soot-particle inception in diffusion flames. *Combust. Flame.*, **100**, 367–375.

Egolfopoulos, F.N., Cho, P., and Law, C.K. 1989. Laminar flame speeds of methane-air mixtures under reduced and elevated pressures. *Combust. Flame.*, **76**, 375–391.

Flavin, C., Sawin, J.L., Mastny, L., Aeck, M.H., Hunt, S., MacEvitt, A., and Stair, P. 2006. *American Energy: The Renewable Path to Energy Security (Paper)*, Worldwatch Institute, Washington, DC.

Gao, X., and Groth, C.P.T. 2006. A parallel adaptive mesh refinement algorithm for predicting turbulent non-premixed combusting flows. *Int. J. Comput. Fluid Dyn.*, **20**(5), 349–357.

Gao, X., Northrup, S.A., and Groth, C.P.T. 2011. Parallel solution-adaptive method for two-dimensional non-premixed combusting flows. *Prog. Comput. Fluid Dyn.*, **11**(2), 76–95.

Goodwin, D.G. 2003. An open-source, extensible software suite for CVD process simulation. *Chemical Vapor Deposition XVI and EUROCVD 14*, 155–162.

Johnson, R.F., VanDine, A.C., Esposito, G.L., and Chelliah, H.K. 2015. On the axisymmetric counterflow flame simulations: Is there an optimal nozzle diameter and separation distance to apply quasi one-dimensional theory? *Combust. Sci. Tech.*, **187**, 37–59.

Korusoy, E., and Whitelaw, J.H. 2001. Opposed jets with small separations and their implications for the extinction of opposed flames. *Exp. Fluids.*, **31**, 111–117.

Li, J., Kazakov, A., Chaos, M., and Dryer, F.L. (2007). Chemical kinetics of ethanol oxidation. In *Proceedings of the 5th us combustion meeting*, san diego, california, u.s.a., March 25–28. (p. 1–17).

Marinov, N. 1999. A detailed kinetic model for high temperature ethanol oxidation. *Int. J. Of Chem. Kin.*, **31**, 183–220.

Roe, P.L. 1981. Approximate Riemann solvers, parameter vectors, and difference schemes. *J. Comput. Phys.*, **43**, 357–372.

Sachdev, J.S., Groth, C.P.T., and Gottlieb, J.J. 2005. A parallel solution-adaptive scheme for predicting multi-phase core flows in solid propellant rocket motors. *Int. J. Comput. Fluid Dyn.*, **19**(2), 159–177.

Sarnacki, B.G., Esposito, G., Krauss, R.H., and Chelliah, H.K. 2012. Extinction limits and associated uncertainties of nonpremixed counterflow flames of methane, ethylene, propylene and n-butane in air. *Combust. Flame.*, **159**, 1026–1043.

Saxena, P., and Williams, F.A. 2007. Numerical and experimental studies of ethanol flames. *Proc. Combust. Inst.*, **31**, 1149–1156.

Seiser, R., Humer, S., Seshadri, K., and Pucher, E. 2007. Experimental investigation of methanol and ethanol flames in nonuniform flows. *Proc. Combust. Inst.*, **31**, 1173–1180.

Seiser, R., Trees, T.D., and Seshadri, K. 1998. Structure and extinction of non-premixed *n*-heptane flames. *Proc. Combust. Inst.*, **27**, 649–657.

Seshadri, K. 2005 May. *Counterflow Extinction of Premixed and Nonpremixed Methanol and Ethanol Flames (Tech. Rep.)*, University of California Energy Institute, 2547 Channing Way, 5180 Berkeley, California 94720-5180.

Seshadri, K., Lu, T., Herbinet, O., Humeer, S., Niemann, U., Pitz, W.J., … Law, C.K. 2009. Experimental and kinetic modeling study of extinction and ignition of methyl decanoate in laminar non-premixed flows. *Proc. Combust. Inst.*, **32**, 1067–1074.

Seshadri, K., and Williams, F.A. 1978. Laminar flow between parallel plates with injection of a reactant at high reynolds number. *Int. J. Heat Mass Trans.*, **21**, 251–253.

Vagelopoulos, C.M., and Egolfopoulos, F.N. 1998. Direct experimental determination of laminar flame speeds. *Proc. Combust. Inst.*, **27**, 513–519.

Wang, W. 2014. Experimental and numerical investigation of structure and extinction limits of biofuels in laminar counterflow diffusion flames. Unpublished master's thesis. University of Toronto.

Weiss, J.M., and Smith, W.A. 1995. Preconditioning applied to variable and constant density flows. *AIAA J.*, **33**(11), 2050–2057.

Williams, B.A. 2001. Sensitivity of calculated extinction strain rate to molecular formulation in non-premixed counterflow flames. *Combust. Flame.*, **124**, 330–333.

Won, S.H., Sun, W., and Ju, Y. 2010. Kinetic effects of toluene blending on the extinction limit of *n*-decane diffusion flames. *Combust. Flame.*, **157**(3), 411–420.

Xia, F., and Axelbaum, R.L. 2013. Simplifying the complexity of diffusion flames through interpretation in C/O ratio space. *Comp. Math. Applic.*, **65**(10), 1625–1632.

Yu, G., Law, C.K., and Wu, C.K. 1986. Laminar flame speeds of hydrocarbon + air mixtures with hydrogen addition. *Combust. Flame.*, **63**, 339–347.